Parallel optical read-out of micromechanical pillars applied to prostate specific membrane antigen detection

Martina Tardivo [a,b,*], Valeria Toffoli [a,c], Giulio Fracasso [d], Daniele Borin [a,c], Simone Dal Zilio [a], Andrea Colusso [e], Sergio Carrato [c], Giacinto Scoles [b], Moreno Meneghetti [e], Marco Colombatti [d], Marco Lazzarino [a]

[a] CNR-IOM, Area Science Park, Basovizza S.S. 14Km 163.5, 34149 Trieste, Italy
[b] University of Udine, Biological and Medical Science, Ospedale della Misericordia, 33100 Udine, Italy
[c] University of Trieste, Piazzale Europa, 34127 Trieste, Italy
[d] Department of Pathology and Diagnostics, University of Verona Policlinico "G.B. Rossi", P.le L. Scuro, 10 37134 Verona, Italy
[e] Nanostructures and Optics Laboratory, Department of Chemical Sciences University of Padova, Via Marzolo 1 35131 Padova, Italy

ARTICLE INFO

Accepted 9 May 2015

Keywords:
Micromechanical sensors
Parallel optical read-out detection
Prostate Specific Membrane Antigen

ABSTRACT

Micro and nanomechanical resonators represent a promising platform for proteins label-free detection because of their extreme sensitivity, fast response and low cost. Micro-pillars are columnar resonators that can be easily arranged in dense arrays of several thousand sensors in a squared mm. To exploit such a large density, however, a method for tracking independently micropillars resonance frequency is required. Here we present a detection method based on CCD imaging and software image analysis, which can measure the resonance frequency of tens of pillars in parallel. Acquiring simultaneously the frequency shift of up to 40 sensors and applying a proper statistical analysis, we were able to overcome the variability of the single measures improving the device sensitivity at low analyte concentration range.

As a proof of concept, this method has been tested for the detection of a tumor marker, the Prostate Specific Membrane Antigen (PSMA). Pillars have been functionalized with an antibody against PSMA. The tumor marker (PSMA) has been detected in a range of concentrations between 300 pM and 100 nM, in buffer and in diluted bovine serum. The sensitivity of our method was limited only by the affinity constant of the antigen–antibody recognition. Moreover, this detection technique demonstrated to be effective in the 1–6 nM range, which is the window of PSMA concentration of clinical interest.

1. Introduction

The application of micro- and nano-electromechanical sensors was proposed at the end of the 1990s and since then experienced a constant development. Two principal strategies have been recognized involving micro and nanocantilevers or double clamped beams. The static deflection mode, in which molecules adsorbed on the sensor surface create an asymmetrical stress that results in sensor bending (Fritz et al., 2000). Instead, in the dynamic mode, the resonance frequency of the sensor is monitored and its variation upon mass adsorption is detected (Battiston et al., 2001). In the latter configuration, the main advantages are: the extremely low limit of mass detection, the small amount of sample required for operation and the label-free detection of molecular species. All these advantages come from the small size of the sensor that is often in the submicron range, thus reducing dramatically the sensor mass and increasing the surface to volume ratio.

In the last decade, applications in different fields were demonstrated (Arlett et al., 2011; Bargatin et al., 2012; Pang et al., 2012; Tamayo et al., 2013): single atom sensitivity was reached in vacuum condition (Yang et al., 2006), applications in air and liquid were proposed, with a detection limit reduced to attogram (10^{-18} g) (Verd et al., 2007) and to nanogram (10^{-9} g) (Braun et al., 2009) respectively.

Micromechanical pillars are vertical cantilevers used as mass sensors in dynamic mode (Kehrbusch et al., 2008; Melli et al., 2010). Because of the reduced lateral size, pillars can be arranged in a dense array; when nearest neighbors are close enough and the lateral surfaces are hydrophobic, a superhydrophobic Cassie–Baxter (CB) state is realized (Melli et al., 2011). When a solution is introduced in a CB pillar array, gas is trapped between the lateral walls and only the top surface of the pillars is in contact with the solution, ensuring that the biochemical recognition process occurs

* Corresponding author at: CNR-IOM, c/o Area Science Park–Basovizza, Build. MM, SS 14Km 163.5 I-34149 Trieste, Italy. Fax: +39 040226767.
E-mail address: tardivo@iom.cnr.it (M. Tardivo).

only on the top. This configuration reduces drastically device deterioration and non specific adsorption which can change not only the cantilever mass but also its stiffness, making measurement interpretation difficult (Tamayo et al., 2013). Moreover, we recently demonstrated that, at low concentration, when the biochemical recognition is diffusion limited rather than reaction limited, if the sensor area is significantly smaller than the analyte diffusion length and the pillar spacing larger, a reduction of incubation times down to three order of magnitude can be obtained (Melli et al., 2011; Nair and Alam, 2006).

Finally, pillars dense arrays can be exploited to implement a multiple sensor. However, the complexity of addressing electrically each individual resonator grows exponentially as the number of pillars increases. On the other hand, if a suitable optical detection scheme is adopted, thousands of pillars, integrated in few mm^2 areas, could be monitored in parallel. This enables sensitivity improvements over individual pillars by averaging signals coming from a multitude of devices in the array.

In this paper we report on an innovative read-out strategy which enables monitoring the frequency resonance of tens of pillars in parallel using a CCD imaging system and software image processing. As proof of principle, we detected a tumor associated antigen of Prostate Cancer (PCa), the Prostate Specific Membrane Antigen (PSMA), both in physiological solution and bovine serum.

2. Material and methods

2.1. Pillars fabrication

Pillars are obtained by a deep dry etching of a patterned Si wafer. Details of the fabrication procedure are reported elsewhere (Borin et al., 2014). Briefly, we started from a well cleaned Si(100) wafer. A 20 nm thick Nickel mask was patterned by electron beam lithography and electron beam evaporation, creating an hexagonal lattice of 2 μm x 3 μm rectangles, corresponding to the top area of the micropillars, with a center-to-center distance of 12 μm. The vertical structure was obtained by Induction Coupled Plasma (ICP) Deep Reactive Ion Etching (DRIE), using a BOSCH™-like approach with SF_6, Ar, and C_4F_8. The number of cycles defines the height of the micropillars (around 12 μm). The recipe was optimized in order to obtain a controlled undercut (approximately 2–3°), that reduces the base of the pillar to almost 700 nm and improves the oscillation amplitude of the resonator. An example of the so fabricated matrix is reported in Fig. 1a. Fig. 1b shows a magnified view of a single pillar with the typical scallops created by the cyclical etching process. In order to increase the sensitive area and the oscillation amplitude, "T" shaped pillars were also fabricated starting from Si(100) wafer coated with a 500 nm thick Si_3N_4 layer, defining a larger top area of 3 μm × 4.5 μm. The fabrication process differs from the one described above for the presence of a last isotropic and selective SF_6 dry etching step which thins the silicon structure but not the topmost Si_3N_4 layer. The resulting structure is exemplified in Fig. 1c. This geometry offers a larger active layer, with only a slight increase of the overall pillar mass, a larger oscillation amplitude and smaller resonance frequency, making them easy to detect at the cost of a slightly lower sensitivity.

Finally the Ni layer was stripped from the top of the pillar, the sample was cleaned in piranha solution, thermally oxidized to relax possible residual stress and a layer of 5 nm Cr/20 nm Au was deposited for further chemical reactions.

The described process results in 5 mm × 5 mm silicon chips with a 300 μm × 300 μm patterned area in the center containing an array of 640 pillars. The obtained chips can be handled with tweezers and mounted on the read-out chamber. The production costs of these devices, also in a prototypal stage, are extremely low, therefore the devices were used as produced and disposed after use.

Finally, in spite of the parallel fabrication process, pillars showed different resonance frequency. This is due to several sources of inhomogeneities in the lithographic process. Arrays of micro- and nano-mechanical resonators were already reported to have a rather broad distribution of resonance frequencies (Bargatin et al., 2012; Martinez et al., 2010; Sampathkumar et al., 2011). A characterization of the pillar resonance frequency distribution is discussed in Supplementary Information S2.

2.2. Pillars hydrophobization

In order to achieve permanent superhydrophobic properties (Cassie–Baxter state), pillar walls were coated with a hydrophobic layer as discussed in detail in (Borin et al., 2014). In particular we formed an alkanosilane coating through octadecyltrichlorosilane (OTS) deposition from a 1 mM solution in dry toluene for 1 h. The

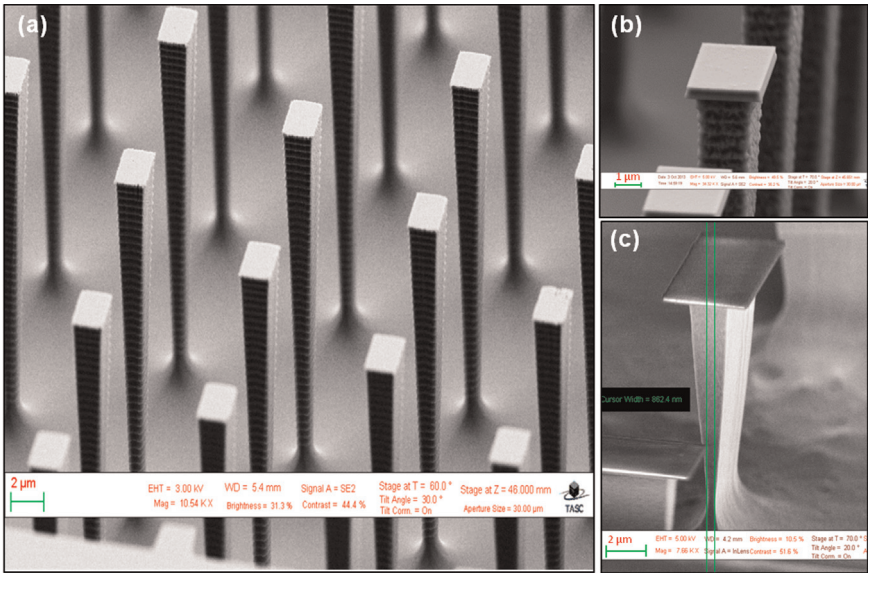

Fig. 1. (a) SEM image of a micropillars array obtained from deep plasma etching of a patterned silicon wafer, the tapered shape is visible. (b) Magnified view of a single pillar with the typical scallops created by the etching process. (c) SEM image of a "T" shaped pillar obtained adding an isotropic and selective dry etching step to the process.

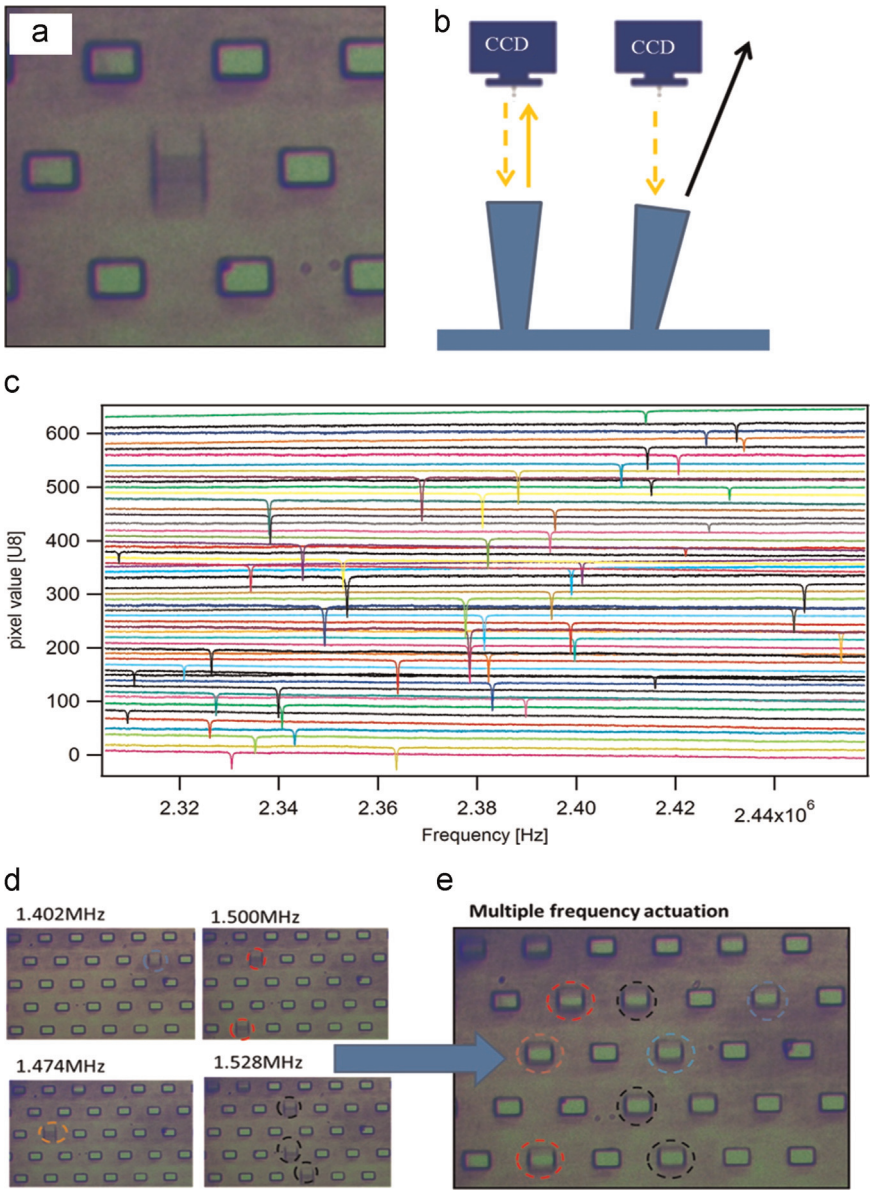

Fig. 2. (a) Optical image of a "T" shaped pillar array actuated by a piezo at the resonance frequency of one of them, in the middle a pillar is oscillating. (b) A schematic representation of pillar detection: when pillars oscillate, the light reflection path is slightly deviated and the light intensity recorded by the CCD slightly decreased. (c) 53 traces corresponding to 53 different pillars as a function of actuation frequency. (d) Individual actuation mode. (e) Multiple actuation mode is obtained driving separate frequencies in parallel through the same piezo actuator and detecting simultaneously more pillars with separate resonance frequencies.

process was performed inside a glovebox saturated with anhydrous nitrogen. After the OTS deposition, fabricated chips were rinsed with toluene, acetone and isopropyl alcohol to remove molecules not chemisorbed on the surface and then dried with a nitrogen flux.

2.3. *Parallel read-out detection method*

The resonance frequency detection was based on the following observation. When the pillars oscillation amplitude is comparable or larger than the optical resolution, the image appears blurred and upon suitable illumination, darker (see Fig. 2a and b). Moreover, the higher the oscillation amplitude, the darker the image. In order to have large enough oscillation amplitudes, the frequency response was measured in a vacuum chamber with a base pressure below 10^{-4} mbar. A proper illumination of the sample was obtained by a modified Köhler illuminator, which consisted of a bulb halogen lamp, an optical fiber and a lens coupled with a long working distance objective (Olympus LMPLANFL 50x/0.5); a cubic beam splitter was used to direct the reflected light on a ½ in. CCD camera (DBK 41BU02).

The pillar images were captured at 15 frames per second (fps) and the image intensity in correspondence of the top of pillar was acquired (see Fig. 2a and b); acquiring image intensity as a function of frequency, the dynamic response of the pillars can be obtained (see Supplementary Video).

Supplementary material related to this article can be found online at http://dx.doi.org/10.1016/j.bios.2015.05.026.

The pillar motion was acoustically excited with a piezoelectric crystal; excitation voltage ranged from 0.5 to 2 VPP and frequency ranged from 1.3 to 1.9 MHz.

The number of pillars that can be measured in parallel depends on the field of view of the imaging system and on the size of the pillars: in our system a maximum of 64 pillars were observed. However, practically, not all the pillars showed an oscillation amplitude large enough and only a subset of those included in the

field of view were measured. Fig. 2c displays 53 traces acquired in parallel corresponding to 53 different pillars in the CCD image.

2.4. Pillar functionalization with D2B-SH

In order to functionalize the pillar sensor against PSMA: i) a layer of Au was evaporated on the pillar top layer immediately before the functionalization procedure; ii) a monoclonal antibody anti-PSMA (D2B) (Colombatti et al., 2010) was functionalized with a thiol group (Selvestrel et al., 2013) to be linked to the Au surface; iii) the chips were incubated for 10 min at room temperature in 20 μL of D2B solution at 70 nM in a vapor saturated environment to avoid droplet drying; iv) the chips were rinsed in PBS, blown dried in N_2 and used for PSMA detection. Following this procedure, and assuming a uniform coverage, we obtained, on the pillar top an active layer of D2B with an areal density of 2×10^{12} mol/cm^2. Additional details regarding optimization of the D2B layer on the top of pillar are reported in the Supplementary Information S1.

Remarkably, volume and concentrations as small as 1 μL and 0.7 nM can be used to functionalize our chip. These conditions compared with those used in a standard immunoassay (100 μL and 1 μM) allowed a reduction of antibody requirement of more than 5 order of magnitude, which could be a great advantage when the availability of antibody is extremely low or the production is expensive.

2.5. PSMA detection

Before exposing the devices to PSMA solution, the surface was incubated for one hour with a blocking agent, bovine serum albumin (BSA), 2%w/v: BSA intercalates between antibodies and saturates all the remaining unspecific adsorption sites.

We performed the detection of a commercial PSMA recombinant protein, r-PSMA, (Cusabio – CN) produced in prokaryotic cells and therefore not glycosylated. The PSMA was diluted in PBS containing 0.2% w/v of BSA (PBS+BSA), or in bovine serum (FCS from Biochrom, Germany) to obtain spiked solutions at the desired concentration. Bovine serum was preferred to human serum, for the absence of any residual unknown concentration of human PSMA that would introduce a systematic error in the sensor characterization. To preserve the superhydrophobicity of the system, bovine serum was diluted 1:20 in PBS (Borin et al., 2014).

The chips functionalized with D2B were incubated for a fixed time in PSMA solution at target concentration, then they were six-fold rinsed in PBS, blown dried in N_2 and loaded in the measurement system.

2.6. Data analysis

Pillar frequency spectra were fitted with a Lorentzian curve using IGOR Pro. The resonance frequency shift was obtained subtracting the peak frequency of Au coated pillar from the peak frequency of the same pillar after biomolecular adsorption. To calculate the molecular density (mol/cm^2) we fixed the pillar sensitivity to 24 Hz/fg and used 150 kDa for the mass of D2B (Colombatti et al., 2010) and 90 kDa for the mass of recombinant-PSMA.

For each sample we measured at least 30 different pillars and we reported the frequency shift mean and standard deviation of the measured values.

One way ANOVA and *t*-student tests were performed by GraphPad prism software, a *p*-Value $p < 0.05$ was considered statistically significant.

3. Results and discussion

3.1. Parallel detection

Sensor arrays represent an efficient strategy to increase the sensitive area and reduce the noise (Sampathkumar et al., 2011). In particular for extremely low analyte concentration, rare binding events are compensated increasing the number of detectors. When the array size becomes large, however, the read-out should be performed in parallel, otherwise the analysis time diverges.

In literature, several parallelization approaches have been proposed for cantilevers. Starting from the optical lever scheme, scanning lasers (Mertens et al., 2005), sample (Martinez et al., 2010) or using multiple lasers sources (Arntz et al., 2003) were proposed. However these approaches suffer of limited speed, low cantilever density, high costs and complexity respectively. Recently, Ekinci's group proposed a near field optical technique (Basarir et al., 2012) and one based on an interferometric effect (Sampathkumar et al., 2011) demonstrating the characterization of tens of sensors. Despite the powerful of these methods, the implementation of the optical setup is often challenging.

Pillar size, few μm squared, imposes the use of high numerical aperture objectives to focus a laser on their top. Therefore, although the frequency response of individual pillars has been characterized by optical lever techniques (Kehrbusch et al., 2008; Melli et al., 2010; Melli et al., 2011), the implementation of laser scanning systems is not straightforward. Moreover, pillars oscillate in the device plane, and thus also interferometric detection cannot be applied. On the other hand, a pillar array can be extremely compact and can be imaged in a single field of view of an optical microscope. Our method offers the possibility of monitoring the frequency response of hundreds of pillars in parallel. In this way the advantages of the pillar approach, namely, faster kinetics, higher sensitivity and reduced analytes volumes (Melli et al., 2011), are further enriched by enabling sensitivity improvements over single pillar resonators by averaging signals coming from a multitude of devices in the array. Moreover, in this configuration, pillars with different resonance frequencies can be actuated simultaneously. Indeed the actuation signal could be formed by a superposition of different frequencies that can be controlled independently. By a careful choice of the actuation signal all the pillars can be driven simultaneously at the resonance frequency and the evolution of the resonance frequency can be tracked in parallel in real time (Figs. 2d and e). Finally the intensity of the light impinging on a single resonator is orders of magnitude lower than in the case of the optical lever, the order of 10^3 W/cm^2 versus the 10^5 W/cm^2 of a 1 mW focused red laser. This would help to reduce the laser heating effect that may be detrimental from both the pillar mechanical properties and the stability of the analyte adsorbed on the pillar active area (Lee et al., 2008).

3.2. PSMA detection in buffer and serum

The effectiveness of the proposed approach was demonstrated by detecting a tumor marker, the Prostate Specific Membrane Antigen (PSMA).

PSMA is a transmembrane protein overexpressed by malignant prostate tumor, whose expression is correlated with disease recurrence (Ross et al., 2003). In particular, PSMA serum level has been proposed to discriminate between men affected by benign prostatic hyperplasia (BPH) and PCa patients, whose PSMA serum level is significantly higher (6 nM) than in BPH (1 nM) (Xiao et al., 2001). However the clinical utility of PSMA was hindered by the lack of suitable assays (Hessels and Schalken, 2013). Enzyme- and fluorescence-based immunosensitive assays require the use of a further secondary antibody, but the available candidates still needs

further development to reach the desired sensitivity. For this reason, a label free technique, such as micromechanical sensor weighing, is still the approach of choice for PSMA detection.

To capture PSMA antigen, our pillars have been functionalized with an antibody anti PSMA, the D2B, recently isolated by some of us (Colombatti et al., 2010; Frigerio et al., 2013; Tykvart et al., 2014). We exploited the high binding capability of D2B which recognizes the extracellular domain of PSMA with a K_D lower than the value of the benchmark Ab J591 (Chang et al., 1999). The D2B layer was formed starting from a 70 nM D2B solution in PBS (antibody density of about 2×10^{12} mol/cm^2). Upon BSA passivation, a further frequency shift of about 500 Hz was observed and we used this frequency value as baseline for the following experiments.

We measured the resonance frequency shift in response to 7 different concentrations of PSMA, ranging from 300 pM to 100 nM, diluted in PBS+BSA. In this first series of measurements we worked in presence of BSA, the most abundant protein in the serum. The devices were prepared as described in paragraph 2.5. For each concentration a new disposable chip was used, thus avoiding any cross contamination effect. The results are displayed in Fig. 3a, where the frequency shifts with respect to bare Au-coated pillars are displayed vs the PSMA concentration. The frequency shift comprises three contributions: D2B, BSA and PSMA. On the right axis, corresponding values of PSMA density are shown. The green line indicates the initial frequency shift due to D2B functionalization, as reported in the Supplementary Information. The orange line indicates the frequency shift induced by BSA passivation. The frequency shift induced at each PSMA concentration is displayed with blue symbols. Moreover, in order to provide consistent results, each PSMA concentration was repeated twice.

With 100 nM PSMA, the highest tested concentration, the net shift calculated is around 900 Hz, which corresponds to a 2×10^{12} mol/cm^2 PSMA molecules, meaning that almost all the antibodies bind one antigen. Reducing the concentration of PSMA to 10 nM only 15% of antibodies bind an antigen. The minimum PSMA concentration that we were able to detected was around 1 nM. The data are fitted with a second order Langmuir adsorption curve providing a $K_D = 18$ nM, about three times greater than the value showed by D2B on the native human PSMA (about $K_D = 6.5$ nM) (Colombatti et al., 2010). However, this discrepancy could be ascribed to a reduced binding capability of D2B versus the

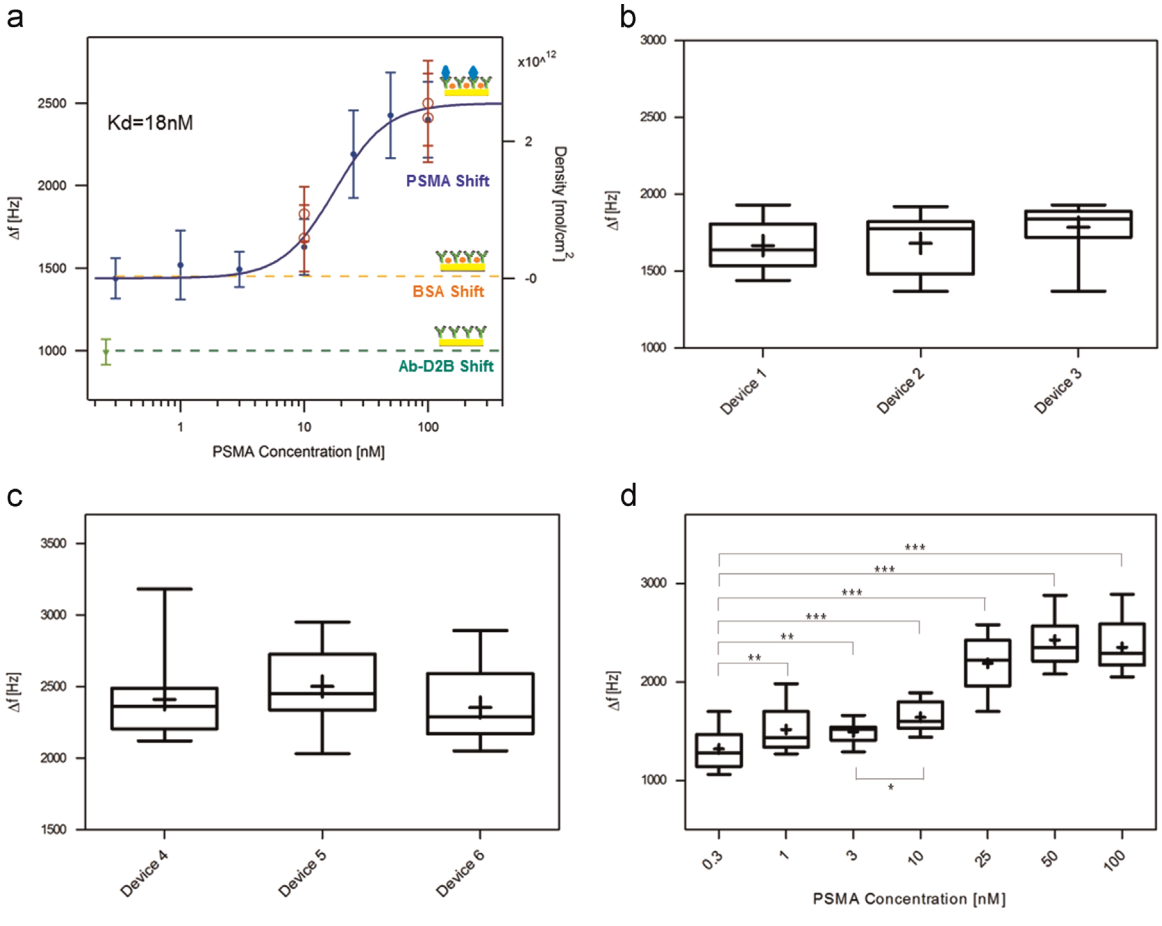

Fig. 3. (a) Results of PSMA detection in PBS, containing BSA 0.2%w/v, with D2B functionalized pillars devices. 7 concentrations, ranging from 300 pM to 100 nM, were tested, full blue circles. On the left axis, frequency shifts induced at each PSMA concentration are displayed. On the right axis, corresponding values of PSMA density are shown. Green line indicates the initial frequency shift occurring after D2B adsorption, while the orange one indicates the frequency shift induced by BSA passivation. Each value is the mean shift and the error bar is the standard deviation of at least 30 independent pillars detected in parallel. Experimental data are fitted with a second order Langmuir curve (blue line) which provides a $K_D = 18$ nM. Red empty circles represent data acquired using three different devices to demonstrate the reproducibility of the detection system. (b) Boxplot representation of data obtained detecting PSMA at 10 nM in PBS containing BSA 0.2%w/v, with D2B functionalized pillars using three different devices. Statistical analysis, one way ANOVA test provides $p = 0.1132$, means and variances are not significantly different (significance $p < 0.05$). (c) Box plot representation of data obtained detecting PSMA in PBS at 100 nM with D2B functionalized pillars using three different devices. Statistical analysis, one way ANOVA test provides $p = 0.1489$, means and variances are not significantly different (significance $p < 0.05$). (d) Box plot representation of data obtained detecting 7 different concentrations of PSMA in PBS containing BSA 0.2%w/v, with D2B functionalized pillars devices; concentrations ranging from 300 pM to 100 nM. Data distributions are compared by t-test (significance $p < 0.05$). Data at 300 pM, assumed as baseline, are compared with all the other concentrations. Data at 3 nM and 10 nM are also compared. Significance is represented for each couple as (*) significant $p \leq 0.05$, (**) very significant $p \leq 0.01$, (***) extremely significant $p < 0.001$. (For interpretation of the references to color in this figure legend, the reader is referred to the web version of this article.)

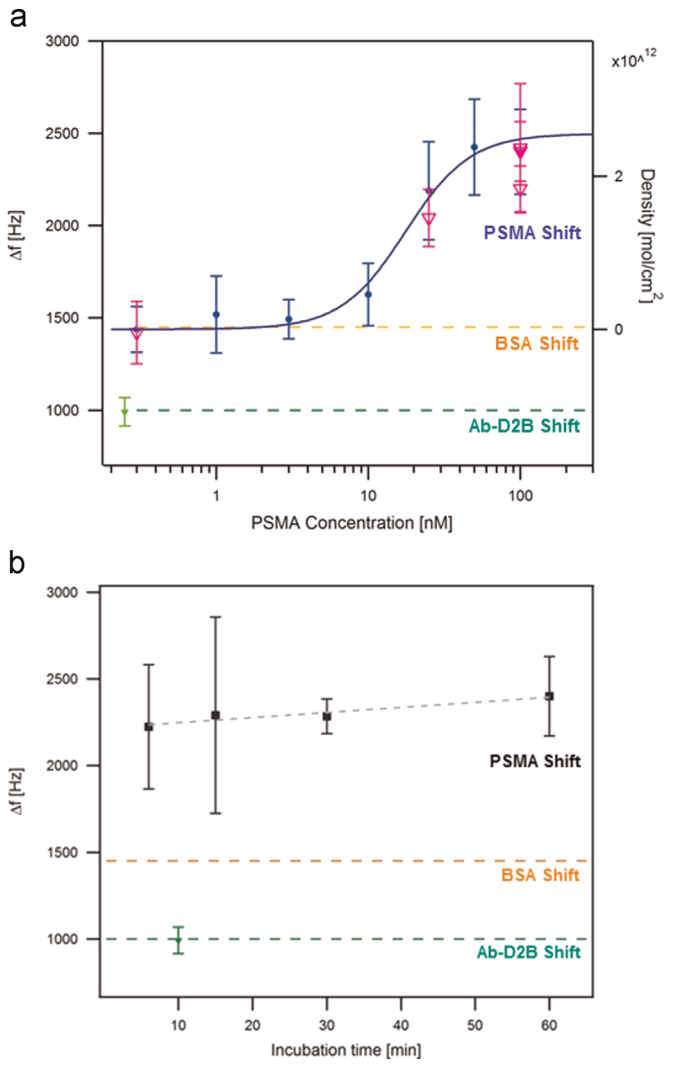

Fig. 4. (a) Results of PSMA detection in diluted bovine serum, with D2B functionalized pillars devices. Full blue circles and blue line are the same already shown in Fig. 3a, empty purple triangles represent data obtained detecting PSMA in diluted bovine serum (1:20 in PBS). Two concentrations, 10 nM and 100 nM, and a control sample (only bovine serum) were tested. (b) Dark squares show frequency shifts induced by PSMA at 100 nM in PBS, containing BSA 0.2%w/v, as a function of the antigen incubation time. (For interpretation of the references to color in this figure legend, the reader is referred to the web version of this article.)

recombinant protein, used in these experiments, with respect of the native one used during the immunization process to generate D2B.

To demonstrate the reproducibility of the system, the detection of PSMA at 10 nM and 100 nM in PBS+BSA was performed using three different chips fabricated in different production batches: these data are shown as red empty circles in Fig. 3a.

Since the output of the pillar array for each PSMA concentration can be seen as a population of identical sensors subject to identical exposure, the results from different concentrations or from different experiments with the same concentration can be statistically compared to evaluate the significance.

For both concentrations, data distributions are reported as box plot in Fig. 3b and c. The agreement among measurements conducted on our replicated devices was analyzed performing an ANOVA test (significance $p < 0.05$) that provided a $p = 0.11$. As result, means are not significantly different or, in other words, the measures are reproducible.

To evaluate the difference in the pillar response, when incubated with different PSMA concentrations, we performed a statistical analysis, *t*-test (significance $p < 0.05$), among data obtained detecting PSMA in PBS+BSA at 7 concentrations (ranging from 300 pM to 100 nM). The analysis showed that all the concentrations tested were from highly significantly ($p < 0.01$) to very highly significantly ($p < 0.001$) different from the baseline, as reported in Fig. 3d. Moreover, *t*-test performed between data obtained for PSMA at 3 nM and 10 nM provided a $p = 0.015$ and confirmed that we are able to distinguish the response at a 3 nM PSMA value (which seems to be associated to the absence of malignancy) from the response at a 10 nM PSMA value (which seems to be associate to the presence of a prostate tumor) (Xiao et al., 2001).

Summarizing, even if single measures have a certain variability due to unspecific absorption, or biological noise, by detecting tens of pillars in parallel, we can focus our attention on the data distribution rather than on individual measures, improving the sensor performances.

To analyze the capability of our device to measure the antigen in physiological conditions, we detected PSMA in diluted bovine serum. We used two PSMA concentrations, 10 nM and 100 nM and a control sample without PSMA. The frequency shifts induced in diluted serum are comparable with the shifts obtained in PBS (data are shown in Fig. 4a). The control sample induced a shift which is comparable with the baseline assumed after BSA passivation, while samples incubation at 10 nM and 100 nM induced shifts slightly lower than in PBS, but still significantly higher than the baseline.

Finally, we performed a set of experiments of PSMA detection in PBS+BSA as function of the incubation time, using a 100 nM PSMA concentration. The results displayed in Fig. 4b show that, by reducing the incubation time by a factor 10, the PSMA detection remains constant within the experimental error. This result is consistent with the previous observations of Melli (Melli et al., 2011) on the dynamics of the formation of a self-assembled monolayer on the pillar surface. The dramatic reduction of the incubation times required to reach surface saturation in the case of micron sized isolated surfaces, is explained in the framework of diffusion limited adsorption as the transition from a 1D diffusion field in the case of extended surfaces, to a 3D diffusion field in the case of micron sized surfaces.

4. Conclusions

We introduced a detection method that allows to monitor the frequency shift of tens of pillars in parallel, which enables to overcome the variability of single measures improving the sensor performances. The application of such system for biomolecular detection was demonstrated through the detection of PSMA antigen on specifically functionalized micropillars. The sensitivity of our method is limited only by the affinity constant of the antigen–antibody recognition and is set in the nM range. Moreover, this approach requires only one recognition event (in contrast to the usual immunosensing assays that require also a secondary antibody), a sample volume as small as 10 μL, an antibody concentration as small as 0.7 nM and greatly reduced incubation times thanks to the sensor small size that involves a 3D diffusion field.

Acknowledgments

This work has been partially funded by the European Research Council under the European Union's Framework Program (FP/2007-2013)/ERC Grant Agreement no. 269051, by the Associazione

Italiana per la Ricerca sul Cancro (AIRC), Special Program Molecular Clinical Oncology, 5 × 1000, (No. 12214) and by Italian Ministry of Education MIUR (FIRB RBAP11ETKA_003).

MC gratefully acknowledges Fondazione Cariverona (Verona Nanomedicine Initiative and Interceptin project), Fondazione Cariverona/AIRC Progetto Regione Veneto and Italian Minister of Health RF-2010-2305526 for supporting this work.

Appendix A. Supplementary material

Supplementary data associated with this article can be found in the online version at http://dx.doi.org/10.1016/j.bios.2015.05.026.

References

Arlett, J.L., Myers, E.B., Roukes, M.L., 2011. Nat. Nanotechnol. 6 (4), 203–215.
Arntz, Y., Seelig, J.D., Lang, H.P., Zhang, J., Hunziker, P., Ramseyer, J.P., Meyer, E., Hegner, M., Gerber, C., 2003. Nanotechnology 14 (1), 86–90.
Bargatin, I., Myers, E.B., Aldridge, J.S., Marcoux, C., Brianceau, P., Duraffourg, L., Colinet, E., Hentz, S., Andreucci, P., Roukes, M.L., 2012. Nano Lett. 12 (3), 1269–1274.
Basarir, O., Bramhavar, S., Ekinci, K.L., 2012. Nano Lett. 12 (2), 534–539.
Battiston, F.M., Ramseyer, J.P., Lang, H.P., Baller, M.K., Gerber, C., Gimzewski, J.K., Meyer, E., Guntherodt, H.J., 2001. Sensor Actuat. B-Chem. 77 (1-2), 122–131.
Borin, D., Melli, M., Dal Zilio, S., Toffoli, V., Scoles, G., Toffoli, G., Lazzarino, M., 2014. Sens. Actuat. B: Chem. 199, 62–69.
Braun, T., Ghatkesar, M.K., Backmann, N., Grange, W., Boulanger, P., Letellier, L., Lang, H.P., Bietsch, A., Gerber, C., Hegner, M., 2009. Nat. Nanotechnol. 4 (3), 179–185.
Chang, S.S., Reuter, V.E., Heston, W.D., Bander, N.H., Grauer, L.S., Gaudin, P.B., 1999. Cancer Res. 59 (13), 3192–3198.
Colombatti, M.F.G., Cingarlini, S., Canevari, S., Figini, M., 2010. In: Verona, U.D.S.D. (Ed.).
Frigerio, B., Fracasso, G., Luison, E., Cingarlini, S., Mortarino, M., Coliva, A., Seregni, E., Bombardieri, E., Zuccolotto, G., Rosato, A., Colombatti, M., Canevari, S., Figini, M., 2013. Eur. J. Cancer 49 (9), 2223–2232.
Fritz, J., Baller, M.K., Lang, H.P., Rothuizen, H., Vettiger, P., Meyer, E., Guntherodt, H., Gerber, C., Gimzewski, J.K., 2000. Science 288 (5464), 316–318.
Hessels, D., Schalken, J.A., 2013. Asian J. Androl. 15 (3), 333–339.
Kehrbusch, J., Ilin, E.A., Hullin, M., Oesterschulze, E., 2008. Appl. Phys. Lett. 93 (2), 023102.
Lee, J., Goericke, F., King, W.P., 2008. Sens. Actuat. A: Phys. 145-146, 37–43.
Martinez, N.F., Kosaka, P.M., Tamayo, J., Ramirez, J., Ahumada, O., Mertens, J., Hien, T. D., Rijn, C.V., Calleja, M., 2010. Rev. Sci. Instrum. 81, 12.
Melli, M., Pozzato, A., Lazzarino, M., 2010. Microelectron. Eng. 87 (5-8), 730–733.
Melli, M., Scoles, G., Lazzarino, M., 2011. ACS Nano 5 (10), 7928–7935.
Mertens, J., Alvarez, M., Tamayo, J., 2005. Appl. Phys. Lett. 87, 23.
Nair, P.R., Alam, M.A., 2006. Appl. Phys. Lett. 88 (23), 233120.
Pang, W., Zhao, H., Kim, E.S., Zhang, H., Yu, H., Hu, X., 2012. Lab. Chip 12 (1), 29–44.
Ross, J.S., Sheehan, C.E., Fisher, H.A., Kaufman Jr., R.P., Kaur, P., Gray, K., Webb, I., Gray, G.S., Mosher, R., Kallakury, B.V., 2003. Clin. Cancer Res.: Off. J. Am. Assoc. Cancer Res. 9 (17), 6357–6362.
Sampathkumar, A., Ekinci, K.L., Murray, T.W., 2011. Nano Lett. 11 (3), 1014–1019.
Selvestrel, F., Moret, F., Segat, D., Woodhams, J.H., Fracasso, G., Echevarria, I.M., Bau, L., Rastrelli, F., Compagnin, C., Reddi, E., Fedeli, C., Papini, E., Tavano, R., MacKenzie, A., Bovis, M., Yaghini, E., MacRobert, A.J., Zanini, S., Boscaini, A., Colombatti, M., Mancin, F., 2013. Nanoscale 5 (13), 6106–6116.
Tamayo, J., Kosaka, P.M., Ruz, J.J., San Paulo, A., Calleja, M., 2013. Chem. Soc. Rev. 42 (3), 1287–1311.
Tykvart, J., Navratil, V., Sedlak, F., Corey, E., Colombatti, M., Fracasso, G., Koukolik, F., Barinka, C., Sacha, P., Konvalinka, J., 2014. The Prostate 74 (16), 1674–1690.
Verd, J., Uranga, A., Abadal, G., Teva, J., Torres, F., Perez-Murano, F., Fraxedas, J., Esteve, J., Barniol, N., 2007. Appl. Phys. Lett. 91, 1.
Xiao, Z., Adam, B.L., Cazares, L.H., Clements, M.A., Davis, J.W., Schellhammer, P.F., Dalmasso, E.A., Wright, G.L., 2001. Cancer Res. 61 (16), 6029–6033.
Yang, Y.T., Callegari, C., Feng, X.L., Ekinci, K.L., Roukes, M.L., 2006. Nano Lett. 6 (4), 583–586.